

# Homodyne detection of coherence and phase shift of a quantum dot in a cavity

MORTEN P. BAKKER,<sup>1,\*</sup> HENK SNIJDERS,<sup>1</sup> WOLFGANG LÖFFLER,<sup>1</sup> AJIT V. BARVE,<sup>2</sup> LARRY A. COLDREN,<sup>2</sup> DIRK BOUWMEESTER,<sup>1,2</sup> AND MARTIN P. VAN EXTER<sup>1</sup>

<sup>1</sup>Huygens-Kamerlingh Onnes Laboratory, Leiden University, P.O. Box 9504, 2300 RA Leiden, The Netherlands

<sup>2</sup>University of California Santa Barbara, Santa Barbara, California 93106, USA

\*Corresponding author: mbakker@physics.leidenuniv.nl

Received 8 April 2015; revised 10 June 2015; accepted 11 June 2015; posted 11 June 2015 (Doc. ID 237480); published 30 June 2015

**A homodyne measurement technique is demonstrated that enables direct observation of the coherence and phase of light that passed through a coupled quantum dot (QD)-microcavity system, which in turn enables clear identification of coherent and incoherent QD transitions. As an example, we study the effect of power-induced decoherence, where the QD transition saturates and incoherent emission from the excited state dominates at higher power. Further, we show that the same technique allows measurement of the quantum phase shift induced by a single QD in the cavity, which is strongly enhanced by cavity quantum electrodynamics effects.** © 2015 Optical Society of America

**OCIS codes:** (000.2190) Experimental physics; (020.0020) Atomic and molecular physics; (020.5580) Quantum electrodynamics; (270.0270) Quantum optics; (270.5580) Quantum electrodynamics; (270.5585) Quantum information and processing.

<http://dx.doi.org/10.1364/OL.40.003173>

Quantum dots (QDs) are artificial atoms in the solid state with potential applications for quantum information [1]. Embedding QDs in high-*Q* microcavities holds promise to implement deterministic logic gates [2], entangle independent photons [3], and couple distant QDs to form a quantum network [4]. Additionally, cavity-enhanced light-matter interactions enable a powerful spectroscopic tool for QD characterization. In the following, we present a straightforward technique to analyze both the coherence as well as the quantum phase shift of light transmitted through a QD-cavity system.

Several techniques have been demonstrated to determine the coherence of the emission of a coherently driven two-level transition in an atomic or molecular system, i.e., resonance fluorescence (RF). These techniques include analyzing the interference between RF and the incident laser itself as a function of polarization, analyzing the time correlation function  $g^{(2)}(t)$  using a Hanbury Brown-Twiss setup, measuring with an interferometer the mutual phase coherence between the coherently

scattered light and a local oscillator, or analyzing the frequency spectrum using a high-finesse scanning Fabry-Perot interferometer [5–8]. Additionally, the phase shift of transmitted light through a cavity with a strongly coupled atom can be determined using a heterodyne setup [9].

Recently, such techniques have been extended to also study QDs in solid-state systems [10–13] and to measure the quantum phase shift induced by a coupled QD-cavity system by analyzing the reflection intensity as a function of output polarization [14], or by interfering light reflected from the QD-cavity system with light reflected from another piece of the sample [15]. In this Letter, we present a homodyne detection technique that enables simultaneous measurement of both coherence and induced phase shift. The technique is relatively straightforward as it requires only one scanning laser and it is mostly fiber-based. It provides complete coherence and phase information as a function of scanning laser detuning.

The setup for the homodyne interference technique is schematically displayed in Fig. 1(a). Light from a scanning laser is first split into two paths with a fiber beam splitter (FBS). One path (with intensity  $I_1 \propto |E_1|^2$ ) is transmitted through the QD-cavity system, while the other path ( $I_2 \propto |E_2|^2$ ) is used as the local oscillator. The two signals are combined using a FBS and the interference signal ( $I \propto |E_1 + E_2|^2$ ) is recorded. The sample under study is an oxide-apertured micropillar with embedded InAs self-assembled QDs, a system that combines QD charge and energy control, access to the intermediate coupling regime, and polarization degenerate cavity modes [16–21]. Access to the full polarization degree of freedom enables us to use free-space polarizing optics (Pol1 and Pol2) to set the input and output polarizations. These are either set to be parallel, or the output is set at orthogonal crossed polarization; we use a combination of a quarter-wave plate and a polarizer to compensate for the small amount of birefringence present in the sample. To match the local oscillator polarization (Pol3) to the output polarization (Pol2), we use a coiled fiber polarization controller. In our setup there is no need for active stabilization and a single scan is recorded in typically a couple of seconds.

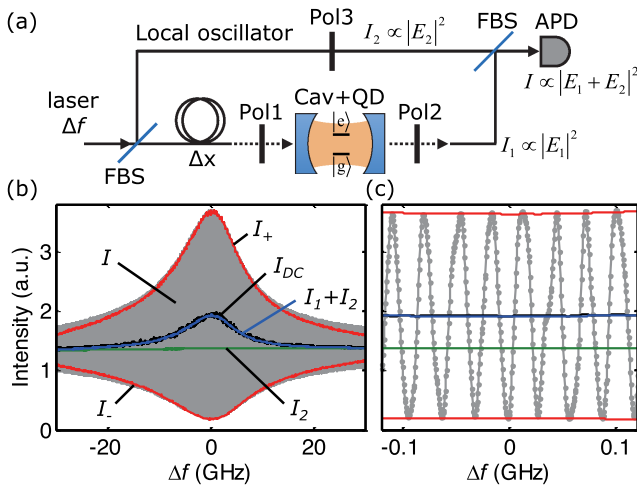


**Fig. 1.** Demonstration of the homodyne interference technique. (a) Schematic of the setup. Coherent light from a scanning laser is split using a fiber beam splitter (FBS), transmitted through the QD-cavity system, recombined with the local oscillator on a FBS and recorded with a avalanche photodiode (APD). Pol, polarization controlling optics. Pol3 is always set to match Pol2. (b) Signal for an empty cavity as function of scanning laser frequency detuning. Gray: interference signal  $I$  when combing the local oscillator and the cavity signal. Black: DC component. Green:  $I_2$  reference signal. Blue: predicted DC signal from the sum  $I_1 + I_2$ . Red: predicted envelope of the interference signal for full interference (see text for details). (c) Zoom-in around zero detuning.

The signal after transmission through the sample is given by  $E_1(t) = E_1 \exp(i\omega t + i2\pi \frac{\Delta x}{c} \Delta f + i\phi(\Delta f, t))$ , where  $\omega$  is the angular frequency,  $\Delta f$  is the laser frequency detuning,  $\Delta x \approx 10$  m is the optical path length difference between the two interferometer arms,  $c$  is the speed of light,  $\phi(\Delta f, t)$  is the phase shift induced by the QD-cavity system, and  $E_1$  is the transmission amplitude of the cavity. When this signal is combined with the local oscillator  $E_2(t) = E_2 e^{i\omega t}$ , the resulting interference intensity  $I$  is given by

$$I = I_1 + I_2 + 2\sqrt{I_1 I_2} \cos\left(2\pi \frac{\Delta x}{c} \Delta f + \phi(\Delta f, t)\right). \quad (1)$$

When the transmitted light is coherent, i.e.,  $\phi(\Delta f, t) = \phi(\Delta f)$  does not vary in time,  $I$  contains interference oscillations that are bounded by  $I_{\pm} = I_1 + I_2 \pm 2\sqrt{I_1 I_2}$ . In the case of incoherent light, which can be interpreted as a rapidly varying phase  $\phi(\Delta f, t)$ , no interference is present and  $I = I_1 + I_2$ .

In Figs. 1(b) and 1(c) we show the case for an empty cavity, where the transmitted light naturally remains fully coherent. Also the polarization is not modified, and we set Pol2 parallel to Pol1 and use a large intensity  $\sim 10 \mu\text{W}$  that is recorded with a fast photodiode instead of an avalanche photodiode. First, we record the reference signal  $I_2$  (green curve) and the transmitted intensity  $I_1$  (not shown) separately; this enables us to predict the DC signal  $I_1 + I_2$  (blue curve) and the interference envelope  $I_{\pm} = I_1 + I_2 \pm 2\sqrt{I_1 I_2}$  (two red curves). The gray curve shows the measured interference signal  $I$ . By low-pass filtering we obtain the DC signal  $I_{DC}$  (black curve) that agrees

well with  $I_1 + I_2$ . The envelope of  $I$  agrees nicely with the independently measured calculated envelopes (red curves), which is especially clear in the zoom-in around the cavity resonance in Fig. 1(c). It is worth pointing out that, even though  $I_1/I_2 \simeq 0.3$ , the ratio of the maxima and minima of the interference fringes is much larger:  $I_+/I_- \simeq 12$ . This demonstrates the beauty of interference and the strength of the technique to measure the coherence of the transmitted light.

We now investigate the coherence properties of light scattered by a charge neutral QD. The lowest excited states of a neutral QD are split in energy, due to electron–hole interaction arising from QD anisotropy, and couple through orthogonally linear polarized transitions with the ground state in a V-type system, as is shown in the inset in Fig. 2(a). We prepare the input polarization at  $45^\circ$  with respect to the polarizations of both transitions such that scattered light, with a polarization of  $0^\circ$  or  $90^\circ$ , passes through the crossed polarizer set to  $-45^\circ$ ; while the cavity background transmission, of which the polarization is unchanged, is filtered out.

Figure 2(a) shows the light scattered by the two transitions for various intensities. First  $I_1$  and  $I_2$  are recorded separately and  $I_1 + I_2$  (blue lines) and the envelope  $I_+$  and  $I_-$  (two red lines) are calculated. The interference signal  $I$  is shown in gray and the low-pass filtered signal  $I_{DC}$  is shown by the black line, which follows the blue line. The interference signal  $I$  was Fourier-filtered with a bandpass filter centered at the oscillation frequency to remove some noise. Figure 2(b) shows a zoom-in of the 500 pW scan around the low-frequency transition. A clear oscillation signal is visible, with a coherent fraction, defined as the ratio  $F = (I_{\max} - I_{\min})/(I_+ - I_-)$ , where  $I_{\max}$  and  $I_{\min}$  are the upper and lower bounds of the interference envelope, of about 0.6. This indicates that the scattered light is only partially coherent.

To investigate this further, we show in Fig. 2(c) the calculated coherent fraction as a function of the laser detuning for various intensities. For a low power of 30 pW it can be seen that the scattered light coherence is about 0.7, but this decreases for increasing intensities. An additional structure of dips in the curve of the coherent fraction becomes visible. This shows that the coherence decreases more rapidly at the QD resonances (marked by the blue vertical lines), compared to the detuned case (the green vertical line marks the center between the two transitions) due to the less efficient off-resonant driving. We note that for increasing power the QD line shapes become distorted and the fine splitting between transitions becomes smaller, due to a dynamical charging effect as is explained in [22].

To analyze this power-dependency, we plot in Figure 2(d) the coherent fraction at the resonance and off the resonance of a QD transition as a function of the laser power. The fraction  $F$  of the scattered light that remains coherent follows the relationship [23]

$$F = \frac{\gamma_{\parallel}/\gamma_{\perp}}{1 + (P/P_0)/(1 + \Delta'^2)}, \quad (2)$$

where  $\gamma_{\parallel}$  and  $\gamma_{\perp}$  denote the population relaxation rate and the homogeneous dephasing rate, respectively,  $P$  is the laser power,  $P_0$  is the saturation power, and  $\Delta'$  is the detuning with respect to the QD linewidth. The scattered light is almost fully

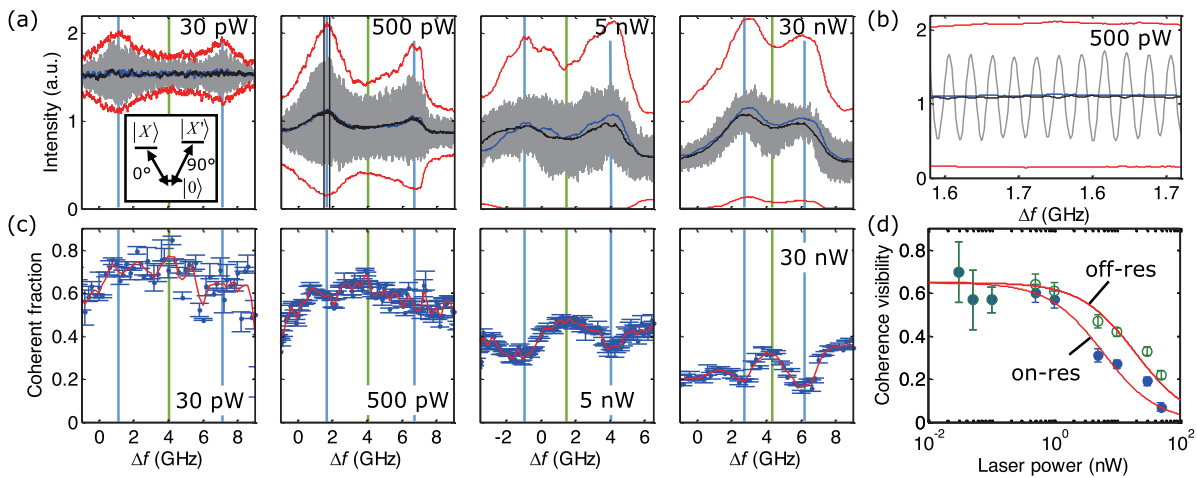


**Fig. 2.** Coherence of the scattered light by a QD as function of laser cavity detuning and injected power. (a) Scans for various laser powers. The input polarization was set to  $45^\circ$  and transmission was recorded through a crossed polarizer such that only the two fine-split QD transitions, see inset for a schematic, and not the cavity are visible. The five curves show:  $I$  (gray),  $I_{DC}$  (black),  $I_1 + I_2$  (blue),  $I_+$  and  $I_-$  (red  $2\times$ ). (b) Zoom-in of the 500 pW scan in (a). (c) Coherent fraction determined as the ratio  $F = (I_{\max} - I_{\min})/(I_+ - I_-)$ . (d) Coherence fraction as function of laser power determined on the resonance of a QD transition [blue vertical lines in (a),(c)] and off resonance (green vertical lines). Red lines are predicted curves using Eq. (2).

coherent if the used power is small and  $\gamma_{\parallel} \approx \gamma_{\perp}$ , i.e., the pure dephasing is small. For increasing power the coherent fraction decreases as the QD excited-state population builds up and incoherent emission increases. For frequencies detuned from the QD resonance the effective driving rate becomes smaller and the effect gets reduced. We show theoretical curves for  $\gamma_{\parallel}/\gamma_{\perp} = 0.65$ ,  $P_0 = 6$  nW, and  $\Delta' = 0$  and  $\Delta' = 1.5$  for the on-resonance and off-resonance cases, which match the data well and demonstrate the nonlinear QD saturation dynamics. The mean intracavity photon number  $\langle \bar{n} \rangle$  is given by  $\langle \bar{n} \rangle = P_{\text{out}}/\kappa_m \hbar \omega$ , where  $\kappa_m \approx 11$  ns<sup>-1</sup> is the mirror loss rate, and the maximum output intensity  $P_{\text{out}} = |t|^2 P$  is a function of the maximum transmittivity  $|t|^2 \approx 0.09$  and incident power  $P$ . A saturation power of  $P_0 = 6$  nW corresponds to a mean intracavity photon number  $\langle \bar{n} \rangle \approx 0.2$ , and sounds reasonable compared to other work with efficient coupling to a single emitter [8]. The direct observation that  $\gamma_{\parallel}/\gamma_{\perp} = 0.65$  indicates that the QD line shape is not only lifetime limited and that additional pure dephasing, such as spectral fluctuations or coupling to phonons, plays a role.

We now turn in Fig. 3 to a negatively charged QD that suffers from decoherence. We use a linear input polarization such that only the light scattered by the circularly polarized QD transitions passes through the crossed output polarizer. In Fig. 3(a) we show  $I_1 + I_2$  (blue line) and the predicted envelope  $I_+$  and  $I_-$  (red lines). The interference signal  $I$  (gray line) now hardly shows oscillations. The calculated coherent fraction, shown by the blue curve in Fig. 3(b), is less than 5%. This implies that  $\gamma_{\parallel}/\gamma_{\perp} \ll 1$  and that the QD suffers from fast decoherence. The green curve in Fig. 3(b) displays the transmitted intensity  $I_1$ ; showing the red detuned QD, and part of the cavity line shape due to the dispersive effect of the QD coupled to it.

The strong incoherent behavior was previously also investigated through high-resolution spectral and polarization

resolved studies in [21]. Here among others a larger homogeneous dephasing rate  $\gamma_{\perp}$  and smaller cooperativity  $C$  were observed for the charged QDs compared to the charge neutral ones. The findings are attributed to a fast cotunneling process of electrons across the very small (20 nm) tunnel barrier that separates the QD from a n-doped contact region. Our technique therefore serves as a powerful QD characterization technique which will help to characterize future sample improvements, such as utilizing a thicker tunnel barrier.

Finally, we show that from the obtained data we can also derive the quantum phase shift induced by a single QD transition coupled to a cavity, which forms a hallmark in cavity quantum electrodynamics (QED) experiments [9,14,15,24]. This phase shift  $\phi(\Delta f)$ , see Eq. (1), can easily be extracted from the interference signal by analyzing the oscillation in a rotating frame, which we realize in practice by multiplying

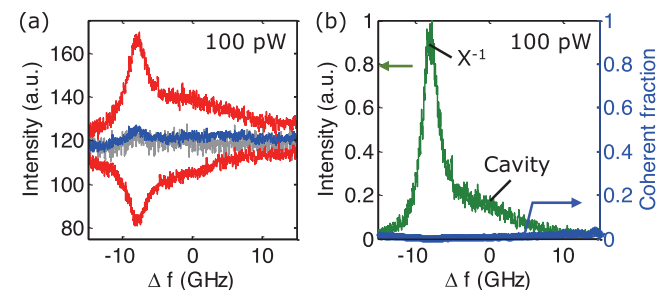


**Fig. 3.** Incoherent scattered light from a singly charged QD ( $X^{1-}$ ) that suffers from fast decoherence. A linear input and a crossed output polarization is used such that only light scattered by the circularly polarized QD transitions is detected. (a) Shows the interference signal  $I$  (gray),  $I_1 + I_2$  (blue), and  $I_+$  and  $I_-$  (red lines). (b) Cross-polarized transmitted intensity  $I_1$  of the QD-cavity system (green) and the determined coherence visibility (blue), showing that the scattered light is nearly fully incoherent ( $F < 0.05$ ).

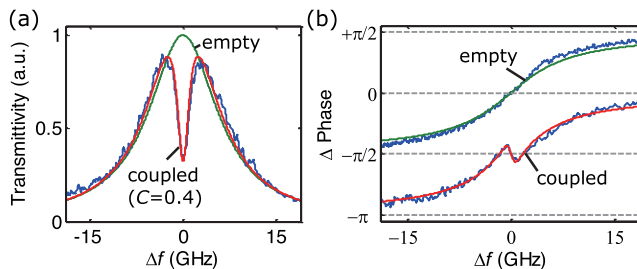


**Fig. 4.** Phase shift induced by a QD-cavity system. (a) shows the transmitted intensity  $I_1$  of a coupled QD-cavity system recorded at  $P_{\text{laser}} = 10 \text{ pW}$ . (b) shows the phase shift for an empty cavity for  $P_{\text{laser}} = 10 \mu\text{W}$  (upper curve) and a coupled system for  $P_{\text{laser}} = 10 \text{ pW}$  (lower curve). The lower curve is displaced for clarity. Red lines in (a) and (b) are predicted curves for QD cooperativity  $C = 0.4$  [21,25–27], QD dephasing rate  $\gamma_{\perp} = 4 \text{ ns}^{-1}$ , and cavity total loss rate  $\kappa = 80 \text{ ns}^{-1}$ . Green curves in (a) and (b) are predicted lines for an empty cavity.

the signal with a complex exponent  $\exp(i2\pi\frac{\Delta x}{c}\Delta f)$  and applying a DC filter. We switch back to a neutral QD and set the input polarization to match one of the fine-split transitions and now record the transmission with a parallel polarization. In Fig. 4(a) we display the transmitted intensity  $I_1$ , showing the QD feature appearing as a dip in the otherwise Lorentzian cavity line shape. Figure 4(b) shows the phase shift induced by an empty cavity and by a coupled QD-cavity system. The red and green curves are calculated based on a cavity QED model with no additional fit parameters [21,26,27], and agree nicely with the data.

In conclusion, we have presented a technique that enables determination of the coherence and the phase of light that is transmitted through a coupled QD-cavity system. The method is simple as it is mostly fiber-based and requires only one scanning laser and standard photodiode detectors. Good signal-to-noise ratio is readily obtained by making the interferometer path difference long using fiber optics; this leads to a high fringe frequency, which relaxes stability requirements strongly. Other methods require movable elements [13], Fabry-Pérot interferometers [11–13], single-photon detection [11,12], or multibeam setups [28]. However, our technique relies on polarization-degenerate cavities enabling cross-polarized detection to access exclusively the light scattered by the QD. This technique is important for QD characterization and for fundamental tests of cavity QED.

**Funding.** FOM-NWO (08QIP6-2); National Science Foundation (NSF) (0901886, 0960331).

**Acknowledgment.** We would like to thank Kier Heeck for stimulating discussions on extracting the QD-induced phase shift and Thomas Ruytenberg for preliminary experimental work.

## REFERENCES

- R. J. Warburton, Nat. Mater. **12**, 483 (2013).
- C. Bonato, F. Haupt, S. S. R. Oemrawsingh, J. Gudat, D. Ding, M. P. van Exter, and D. Bouwmeester, Phys. Rev. Lett. **104**, 160503 (2010).
- C. Y. Hu, W. J. Munro, and J. G. Rarity, Phys. Rev. B **78**, 125318 (2008).
- H. J. Kimble, Nature **453**, 1023 (2008).
- H. J. Kimble, M. Dagenais, and L. Mandel, Phys. Rev. Lett. **39**, 691 (1977).
- T. Basché, W. E. Moerner, M. Orrit, and H. Talon, Phys. Rev. Lett. **69**, 1516 (1992).
- T. Plakhotnik and V. Palm, Phys. Rev. Lett. **87**, 183602 (2001).
- G. Wrigge, I. Gerhardt, J. Hwang, G. Zumofen, and V. Sandoghdar, Nat. Phys. **4**, 60 (2008).
- Q. A. Turchette, C. J. Hood, W. Lange, H. Mabuchi, and H. J. Kimble, Phys. Rev. Lett. **75**, 4710 (1995).
- A. Muller, E. B. Flagg, P. Bianucci, X. Y. Wang, D. G. Deppe, W. Ma, J. Zhang, G. J. Salamo, M. Xiao, and C. K. Shih, Phys. Rev. Lett. **99**, 187402 (2007).
- A. Nick Vamivakas, Y. Zhao, C.-Y. Lu, and M. Atature, Nat. Phys. **5**, 198 (2009).
- E. B. Flagg, A. Muller, J. W. Robertson, S. Founta, D. G. Deppe, M. Xiao, W. Ma, G. J. Salamo, and C. K. Shih, Nat. Phys. **5**, 203 (2009).
- K. Konthasinghe, J. Walker, M. Peiris, C. K. Shih, Y. Yu, M. F. Li, J. F. He, L. J. Wang, H. Q. Ni, Z. C. Niu, and A. Muller, Phys. Rev. B **85**, 235315 (2012).
- I. Fushman, D. Englund, A. Faraon, N. Stoltz, P. Petroff, and J. Vučković, Science **320**, 769 (2008).
- A. B. Young, R. Oulton, C. Y. Hu, A. C. T. Thijssen, C. Schneider, S. Reitzenstein, M. Kamp, S. Höfling, L. Worschech, A. Forchel, and J. G. Rarity, Phys. Rev. A **84**, 011803 (2011).
- N. G. Stoltz, M. Rakher, S. Strauf, A. Badolato, D. D. Lofgreen, P. M. Petroff, L. A. Coldren, and D. Bouwmeester, Appl. Phys. Lett. **87**, 031105 (2005).
- S. Strauf, N. G. Stoltz, M. T. Rakher, L. A. Coldren, P. M. Petroff, and D. Bouwmeester, Nat. Photonics **1**, 704 (2007).
- M. T. Rakher, N. G. Stoltz, L. A. Coldren, P. M. Petroff, and D. Bouwmeester, Phys. Rev. Lett. **102**, 097403 (2009).
- C. Bonato, D. Ding, J. Gudat, S. Thon, H. Kim, P. M. Petroff, M. P. van Exter, and D. Bouwmeester, Appl. Phys. Lett. **95**, 251104 (2009).
- M. P. Bakker, A. V. Barve, A. Zhan, L. A. Coldren, M. P. van Exter, and D. Bouwmeester, Appl. Phys. Lett. **104**, 151109 (2014).
- M. P. Bakker, A. V. Barve, T. Ruytenberg, W. Löfller, L. A. Coldren, D. Bouwmeester, and M. P. van Exter, Phys. Rev. B **91**, 115319 (2015).
- M. P. Bakker, T. Ruytenberg, W. Löfller, A. V. Barve, L. Coldren, M. P. van Exter, and D. Bouwmeester, “Quantum dot nonlinearity through cavity-enhanced feedback with a charge memory,” arXiv:1503.08142 (2015).
- R. Loudon, *The Quantum Theory of Light* (Oxford Science Publications), 3rd ed. (Oxford University, 2000).
- C. Sames, H. Chibani, C. Hamsen, A. Altin, P. T. Wilk, and G. Rempe, Phys. Rev. Lett. **112**, 043601 (2014).
- V. Loo, C. Arnold, O. Gazzano, A. Lemaître, I. Sagnes, O. Krebs, P. Voisin, P. Senellart, and L. Lanco, Phys. Rev. Lett. **109**, 166806 (2012).
- A. Auffèves-Garnier, C. Simon, J.-M. Gérard, and J.-P. Poizat, Phys. Rev. A **75**, 053823 (2007).
- E. Waks and J. Vuckovic, Phys. Rev. Lett. **96**, 153601 (2006).
- F. Masia, N. Accanto, W. Langbein, and P. Borri, Phys. Rev. Lett. **108**, 087401 (2012).